

# NMR Study of CO<sub>2</sub> Capture by Butylamine and Oligopeptide KDDE in Aqueous Solution: Capture Efficiency and Gibbs Free Energy of the Capture Reaction as a Function of pH\*\*

Kaidi Yang,<sup>[a, b]</sup> Joseph Schell,<sup>[a, b]</sup> Fabio Gallazzi,<sup>[c]</sup> Wei Wycoff,<sup>[b]</sup> and Rainer Glaser\*<sup>[a, b]</sup>

We have been interested in the development of rubisco-based biomimetic systems for reversible CO<sub>2</sub> capture from air. Our design of the chemical CO<sub>2</sub> capture and release (CCR) system is informed by the understanding of the binding of the activator CO<sub>2</sub> (<sup>4</sup>CO<sub>2</sub>) in rubisco (ribulose-1,5-bisphosphate carboxylase/oxygenase). The active site consists of the tetrapeptide sequence Lys-Asp-Asp-Glu (or KDDE) and the Lys sidechain amine is responsible for the CO<sub>2</sub> capture reaction. We are studying the structural chemistry and the thermodynamics of CO<sub>2</sub> capture based on the tetrapeptide CH<sub>3</sub>CO-KDDE-NH<sub>2</sub> ("KDDE") in aqueous solution to develop rubisco mimetic CCR systems. Here, we report the results of <sup>1</sup>H NMR and <sup>13</sup>C NMR analyses of CO<sub>2</sub> capture by butylamine and by KDDE. The carbamylation of butylamine was studied to develop the NMR method and with the protocol established, we were able to quantify the oligopeptide carbamylation at much lower concentration. We performed a pH profile in the multi equilibrium system and measured amine species and carbamic acid/carbamate species by the integration of <sup>1</sup>H NMR signals as a

function of pH in the range 8 ≤ pH ≤ 11. The determination of ΔG<sub>1</sub>(R) for the reaction R-NH<sub>2</sub> + CO<sub>2</sub> ⇌ R-NH-COOH requires the solution of a multi-equilibrium equation system, which accounts for the dissociation constants K<sub>2</sub> and K<sub>3</sub> controlling carbonate and bicarbonate concentrations, the acid dissociation constant K<sub>4</sub> of the conjugated acid of the amine, and the acid dissociation constant K<sub>5</sub> of the alkylcarbamic acid. We show how the multi-equilibrium equation system can be solved with the measurements of the daughter/parent ratio X, the knowledge of the pH values, and the initial concentrations [HCO<sub>3</sub><sup>-</sup>]<sub>0</sub> and [R-NH<sub>2</sub>]<sub>0</sub>. For the reaction energies of the carbamylations of butylamine and KDDE, our best values are ΔG<sub>1</sub>(Bu) = -1.57 kcal/mol and ΔG<sub>1</sub>(KDDE) = -1.17 kcal/mol. Both CO<sub>2</sub> capture reactions are modestly exergonic and thereby ensure reversibility in an energy-efficient manner. These results validate the hypothesis that KDDE-type oligopeptides may serve as reversible CCR systems in aqueous solution and guide designs for their improvement.

## Introduction

The atmospheric concentration of CO<sub>2</sub> has been monitored at Mauna Loa Observatory in Hawaii since 1958. This monitoring project has since expanded to incorporate monitoring sites in Alaska, American Samoa, and Antarctica, so as to monitor the global atmospheric CO<sub>2</sub> concentration. As of June 2021, the concentration of CO<sub>2</sub> in the atmosphere at the Mauna Loa site has reached 418.94 ppm and the globally-averaged surface CO<sub>2</sub> concentration is close to 409 ppm.<sup>[1,2]</sup> Drastic cutbacks on CO<sub>2</sub>

emissions are likely not sufficient to bring global climate change under control.<sup>[3-5]</sup> Thus, there is a need for the development of negative emissions technology, and a large part of the overall CO<sub>2</sub> extraction will be from the capture of carbon dioxide from ambient air.<sup>[6-8]</sup> However, current negative emissions technologies will not be sufficient nor economically viable.<sup>[9-13]</sup> The kinetics of amine-based CO<sub>2</sub> capture has been well studied<sup>[14-18]</sup> and aqueous amines are currently used for capturing CO<sub>2</sub> at concentrated sources.<sup>[19-22]</sup> Kortunov et al.<sup>[23]</sup> recently reported a thorough investigation of the capture of CO<sub>2</sub> by several aqueous amines, with varying pK<sub>a</sub> values, by <sup>13</sup>C NMR and included time-dependence and equilibrium distribution information. They suggested that although the solution uptake of CO<sub>2</sub> per load cycle is higher for stronger bases, a weak base capture system could theoretically capture more efficiently by utilizing more load cycles. The efficiency is two-fold in that the facile release reaction takes less energy to remove the CO<sub>2</sub> and the lower temperatures will cause far less degradation of the starting materials than current capture systems.

We have been interested in developing rubisco-inspired systems for reversible CO<sub>2</sub> capture from ambient air.<sup>[24-26]</sup> Ribulose-1,5-bisphosphate carboxylase/oxygenase (rubisco) is the enzyme responsible for most of the carbon fixation of CO<sub>2</sub> from air.<sup>[27]</sup> The active site of rubisco contains the amino group

[a] Dr. K. Yang, Dr. J. Schell, Prof. R. Glaser  
Department of Chemistry,  
Missouri University of Science and Technology  
Rolla, Missouri, 65409 (USA)  
E-mail: glaser@umsystem.edu

[b] Dr. K. Yang, Dr. J. Schell, Dr. W. Wycoff, Prof. R. Glaser  
Department of Chemistry,  
University of Missouri  
Columbia, Missouri, 65211 (USA)

[c] Dr. F. Gallazzi  
Molecular Interaction Core  
University of Missouri  
Columbia, Missouri, 65211 (USA)

[\*\*] KDDE: Tetrapeptide CH<sub>3</sub>CO-KDDE-NH<sub>2</sub>

Supporting information for this article is available on the WWW under <https://doi.org/10.1002/cphc.202300053>



right) between the terminal amino acid aspartic acid and lysine. Both oligopeptides were synthesized and purified, and their NMR spectra were completely assigned. Our measurements allow for the determination of the Gibbs free energy for the formation of the carbamic acids  $\Delta G_1$  and we describe a rigorous treatment of the multi-equilibrium scenarios. Uncertainties in the acidity constants are addressed to estimate error bars for the  $\Delta G_1$  measurements.

## Results and Discussion

### $^1\text{H}$ and $^{13}\text{C}$ NMR Spectra of KDDE in Aqueous Solution

The  $^1\text{H}$  NMR and  $^{13}\text{C}$  NMR spectra of pure KDDE in aqueous solution are shown in Figure 2 and Figure 3, respectively. Both spectra were completely assigned based on extensive 2D-NMR measurements, the assignments are summarized in Table 1 and Table 2. Scheme 3 shows the labelling used for the signal assignments. In each amino acid, the backbone carbon and hydrogen atoms are denoted as  $\alpha$  and the sidechain C and H atoms are named from  $\beta$ . The hydrogen atoms in the backbone amide groups are denoted as "Am. H".

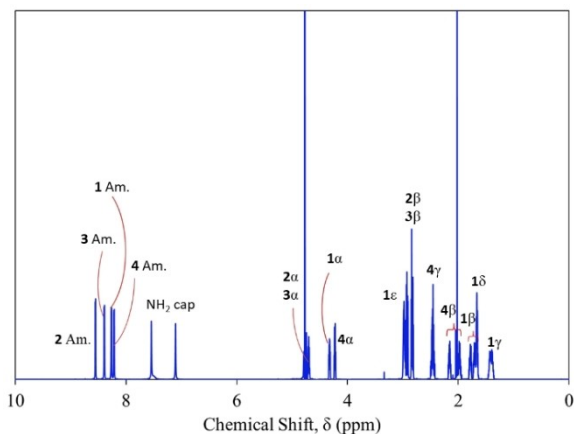


**Figure 2.**  $^1\text{H}$  NMR spectrum of Ac-Lys-Asp-Asp-Glu- $\text{NH}_2$  (KDDE) in 90%  $\text{H}_2\text{O}$  and 10%  $\text{D}_2\text{O}$ .

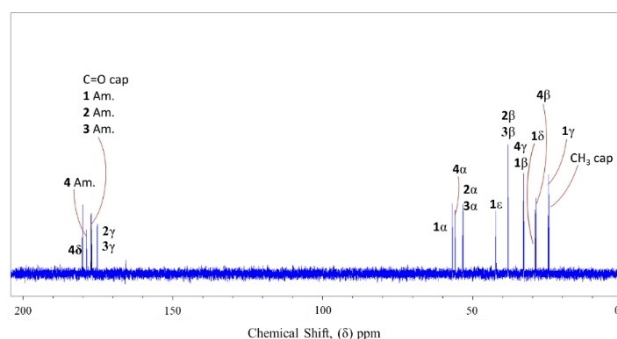


**Figure 3.**  $^{13}\text{C}$  NMR spectrum of Ac-Lys-Asp-Asp-Glu- $\text{NH}_2$  (KDDE) in 90%  $\text{H}_2\text{O}$  and 10%  $\text{D}_2\text{O}$ .

**Table 1.**  $^1\text{H}$  NMR assignments of KDDE and the bridged DPSG-KDDE-GSPK in 90%  $\text{H}_2\text{O}$ , 10%  $\text{D}_2\text{O}$  solution.<sup>[a]</sup>

Residue	Assignment	KDDE			KDDE in f3		
		Min	Max	Split <sup>[b]</sup>	Min	Max	Split
Lys-1	$\text{CH}_3$ -Cap	2.02		s	1.98		s
	1-Amide	8.26	8.27	6.32	8.27		amb.
	1 $\alpha$	4.22	4.24	m	4.19	4.23	m
	1 $\beta$ (2)	1.70	1.73	m	1.67	1.74	m
		1.76	1.81	m	1.76	1.85	m
	1 $\gamma$ (2)	1.37	1.45	m	1.44	1.53	m
	1 $\delta$ (2)	1.65	1.68	m	1.61	1.66	m
	1 $\epsilon$ (2)	2.98		s	3.13	3.17	m
	1 $\zeta$ ( $\text{NH}_3^+$ )	7.51					
Asp-2 <sup>[c]</sup>	2-Amide	8.55	8.56	7.18	8.50	8.51	7.34
	2 $\alpha$	4.68	4.72	m	4.94	4.97	m
	2 $\beta$ (2)	2.81	2.85	m	2.58	2.62	m
		2.91	2.94	m	2.75	2.79	m
Asp-3	2 $\gamma$	dep.					
	3-Amide	8.39	8.40	7.69	8.29	8.31	7.41
	3 $\alpha$	u.w.			4.65	4.67	m
	3 $\beta$ (2)	2.81	2.85	m	2.83	2.87	m
Glu-4		2.91	2.94	m	2.90	2.93	m
	3 $\gamma$	dep.					
	4-Amide	8.21	8.22	7.36	8.23	8.24	6.79
	4 $\alpha$	4.31	4.34	m	4.32	4.36	m
	4 $\beta$ (2)	1.95	2.00	m	2.01	2.05	m
		2.15	2.18	m	2.13	2.20	m
	4 $\gamma$ (2)	2.42	2.50	m	2.46	2.49	m
	4 $\delta$	dep.					
$\text{NH}_2$ -Cap	7.11		s				
Acetate	7.54		s				

[a] All values reported in ppm relative to DSS. dep. = deprotonated, u.w. = under water, amb. = ambiguous. [b]  $^3J_{\text{NH-CH}}$  values are given in Hz. [c] Asp2 and Asp3 signals are not clearly distinct from each other.

**Table 2.**  $^{13}\text{C}$  NMR assignments of KDDE and the bridged DPSG-KDDE-GSPK in 90%  $\text{H}_2\text{O}$ , 10%  $\text{D}_2\text{O}$  solution.<sup>[a]</sup>

Residue	Assignment	KDDE	KDDE in f3
Lys-1	$\text{CH}_3$ -Cap	24.40	24.28
	C=O-Cap	177.29	
	1-Amide	176.92	176.91
	1 $\alpha$	56.63	56.40
	1 $\beta$	33.01	33.32
	1 $\gamma$	24.66	30.52
	1 $\delta$	29.08	29.00
	1 $\epsilon$	42.14	42.07
	Asp-2 <sup>[b]</sup>	2-Amide	
2 $\alpha$		53.04	51.53
2 $\beta$		38.11	39.74
2 $\gamma$		175.01	173.95
Asp-3	3-Amide		
	3 $\alpha$		53.27
	3 $\beta$	38.11	37.99
	3 $\gamma$	175.09	
Glu-4	4-Amide	178.64	175.18
	4 $\alpha$	55.78	
	4 $\beta$	28.74	28.27
	4 $\gamma$	32.86	33.80
	4 $\delta$	180.02	179.89

[a] All values reported in ppm relative to DSS and all are singlets. [b] Asp2 and Asp3 signals are not clearly distinct from each other.

The  $^1\text{H}$  NMR spectrum of KDDE is shown in Figure 2. The signals of the amide hydrogens appear at the range of 8–9 ppm, and each appears as a doublet because of coupling to

their neighboring  $\alpha$  hydrogens ( $^3J_{\text{NH-CH}}$ ). The signals with the chemical shifts of 7.5 and 7.1 ppm are caused by the  $\text{NH}_2$  cap. The  $\alpha$  hydrogens of each amino acid residue give rise to signals in the range of 4–5 ppm. Each  $\alpha$  hydrogen is split by one amide hydrogen and two  $\beta$  hydrogens with different coupling constants, thus causing a multiplet. The region from 1.5 to 3.5 ppm contains all other H peaks and their assignments required 2D-NMR spectroscopy.

Total Correlation Spectroscopy (TOCSY)<sup>[35]</sup> was used to determine which proton signals correlated with each amino acid. For KDDE, the spin network for Lys clearly showed 6 signals (amide,  $\alpha$ ,  $\beta$ ,  $\gamma$ ,  $\delta$ ,  $\epsilon$ ), Glu clearly gave 5 signals (amide,  $\alpha$ ,  $2 \times \beta$ ,  $\gamma$ ), and Asp clearly gave 3 signals (amide,  $\alpha$ ,  $\beta$ ), thus it was straightforward to determine which peaks belonged to which amino acid. Then the position ( $\alpha$ ,  $\beta$ , etc.) was assigned by comparison to reference spectra.<sup>[36]</sup>  $^1\zeta(\text{NH}_3^+)$  is seen as a small shoulder at 7.51 ppm in the  $^1\text{H}$  spectrum. This shoulder shows cross peaks with the  $1\delta$  and  $1\epsilon$  hydrogens in the TOCSY spectrum.

Asp-2 and Asp-3 were difficult to distinguish. The amide proton of Asp-2 was ultimately assigned based on its Nuclear Overhauser Effect Spectroscopy (NOESY)<sup>[37]</sup> signal with the lysine  $\alpha$  proton. The  $\beta$  protons of both Asp residues are diastereotopic and nonequivalent, and their intrinsic difference exceeds the difference between Asp 2 and Asp3. Thus, the signals at 2.81–2.85 are due to one  $\beta$  proton in Asp-2 and one  $\beta$  proton in Asp-3, and likewise the signals at 2.91–2.95 are due to the other  $\beta$  protons in Asp-2 and Asp-3. This explanation is consistent with the TOCSY spectrum, which shows that both  $\beta$  regions overlap with the  $\alpha$ -CH signals and the amide-H signals of both Asp 2 and Asp 3. The  $\text{CH}_3$ -cap and  $\text{NH}_2$ -cap signals were assigned because of their lack of TOCSY cross peaks.

In both Lys and Glu residue, the two  $\beta$  hydrogens are nonequivalent and each  $\beta$  hydrogen couples with one  $\alpha$  H, one  $\beta$  H, and two  $\gamma$  Hs, thus giving rise to a multiplet. The signal of  $4\gamma$  Hs appears more downfield than the  $4\beta$  H signal because it is connected to a carboxylic group; the modest nonequivalence of the  $4\gamma$  H manifest itself in the formation of the multiplet (rather than a triplet) resulting from coupling with the two  $\beta$  Hs. The  $1\gamma$  Hs and  $1\delta$  Hs appear in the range of 1.3–1.8 ppm and the Hs of both methylene groups give rise to multiplets because each hydrogen couples with four non-equivalent hydrogens. The  $1\epsilon$  H signal appears more downfield and it is overlapping with the  $\beta$  H signals of the two Asp residues.

The  $^{13}\text{C}$  NMR spectrum of KDDE is shown in Figure 3. The carbonyl carbons of the amide groups (Am. in Figure 3) and of the side chain carboxylate carbons ( $2\gamma$ ,  $3\gamma$ ,  $4\delta$ ) give rise to signals in the range of 175 to 185 ppm. The signals of  $\alpha$  carbons appear between 50 and 60 ppm, and the signals of  $\beta$  carbons appear between 25 and 50 ppm. With the fully assigned  $^1\text{H}$  spectrum, the assignment of the carbon signals was straightforward. The Heteronuclear Multiple Quantum Correlation (HMQC)<sup>[38]</sup> spectrum was used to identify the side chain and backbone carbon signals and Heteronuclear Multiple Bond Correlation (HMBC)<sup>[39]</sup> spectroscopy allowed the assignments of the carbonyl signals. The carboxyl C signals for Asp-2 and Asp-3 were difficult to distinguish because of the overlap of the  $\beta$  H

signals of Asp-2 and Asp-3 (vide supra). The  $^{13}\text{C}$  signals at 53.0 and 53.2 ppm showed no cross peaks in the HMQC spectrum because the corresponding  $^1\text{H}$  signals were too close to the water peak at 4.7 ppm. However, these signals appear much more clearly in the Heteronuclear Correlation Spectroscopy (HETCOR)<sup>[40]</sup> experiment and could be assigned as the Asp  $\alpha$  signals.

### $^1\text{H}$ and $^{13}\text{C}$ NMR Spectra of Butylamine in Aqueous Solution

The atom numbering of butylamine is defined in Scheme 2. Figure S1 in S11 shows the  $^1\text{H}$  NMR spectrum of butylamine in aqueous solution and peaks occur at 2.61 ppm ( $\alpha$ ), 1.40 ppm ( $\beta$ ), 1.30 ppm ( $\gamma$ ), and 0.88 ppm ( $\delta$ ). Figure S2 in S11 shows the  $^{13}\text{C}$  NMR spectrum of the same sample with peaks at 43.09 ppm ( $\alpha$ ), 36.43 ppm ( $\beta$ ), 22.08 ( $\gamma$ ) and 15.89 ppm ( $\delta$ ). These peaks closely agree with the respective spectra measured in  $\text{CDCl}_3$  solution.<sup>[41]</sup>

### pH Profile of Butylamine Species in the Capture Reaction

The pH of the initial solution was 10.10. This bulk solution of the butylamine/ bicarbonate was distributed into 10 small vials, each holding 20 mL of solution. The pH was adjusted in each individual vial using small aliquots of 3 M  $\text{H}_2\text{SO}_4$  or 1 M NaOH such that the added volume of acid/base did not significantly affect the butylamine concentration. These samples were allowed to equilibrate without venting at room temperature for > 48 hours and the pH was monitored over time (Table 3). NMR spectra were recorded once the pH values became steady and, as can be seen in Table 3, the pH values measured directly before and after the NMR measurements remained essentially the same. The data is reported for the pH values of the samples

**Table 3.** pH Measurements of butylamine and KDDE carbamylation equilibria over time.

Sample	Acid/Base Added [ $\mu\text{L}$ ]	pH $t=0$ s	Before NMR	After NMR	
<b>BuNH<sub>2</sub></b>	3 M $\text{H}_2\text{SO}_4$				
	1	0	10.11	9.95	9.97
	2	25	9.89	9.81	9.81
	3	50	9.58	9.62	9.61
	4	75	9.14	9.38	9.39
	5	100	8.53	8.68	8.70
6	150	7.38	7.57	7.82	
	1 M NaOH				
	7	50	10.30	10.27	10.28
	8	150	10.65	10.66	10.67
	9	200	10.88	10.90	10.90
10	275	11.28	11.26	11.25	
<b>KDDE</b>	3 M NaOH				
	1	15	9.32		9.19
	2	25	9.52		9.41
	3	40	9.78		9.67
	4	80	10.28		10.16
	5	110	10.70		10.56
	6	130	10.82		10.81
7	150	11.21		11.18	

**Table 4.** pH Profile (zgpgppr) of butylamine in 90% H<sub>2</sub>O:10% D<sub>2</sub>O solution with added NaHCO<sub>3</sub>; <sup>1</sup>H NMR spectra.<sup>[a]</sup>

Assign.	pH = 11.25			pH = 10.90			pH = 10.67			pH = 10.28			pH = 9.97		
	δ	Mult.	J	δ	Mult.	J	δ	Mult.	J	δ	Mult.	J	δ	Mult.	J
<b>Parent</b>															
α	2.71	t	7.23	2.78	t	7.29	2.84	t	7.38	2.91	t	7.44	2.94	t	7.50
β	1.46	p	7.38	1.50	p	7.44	1.54	p	7.47	1.58	p	7.47	1.59	p	7.53
γ	1.32	sx	7.47	1.32	sx	7.50	1.35	sx	7.48	1.36	sx	7.54	1.37	sx	7.50
δ	0.89	t	7.38	0.89	t	7.41	0.90	t	7.35	0.91	t	7.41	0.91	t	7.41
<b>Daughter</b>															
α	2.99	q	6.64 <sup>[b,c]</sup>	2.99	q	6.64	2.99	q	6.62	2.99	q	6.62	2.99	q	6.62
β	1.40	m	7.36	1.41	m	7.25	1.41	m	7.26	1.41	m	7.15	1.43	m	7.11
γ							1.30	m	7.47	1.31	m	7.36	1.30	m	7.44
δ				0.88	t	7.29	0.88	t	7.35	0.88	t	7.35	0.88	t	7.38
<b>Assign.</b>															
pH = 9.81			pH = 9.61			pH = 9.39			pH = 8.70			pH = 7.82			
<b>Parent</b>															
α	2.95	t	7.53	2.97	t	7.53	2.97	t	7.53	2.99	t	7.53	2.99	t	7.56
β	1.60	p	7.55	1.61	p	7.56	1.62	p	7.56	1.62	p	7.58	1.62	p	7.56
γ	1.37	sx	7.50	1.37	sx	7.53	1.37	sx	7.53	1.38	sx	7.37	1.38	sx	7.49
δ	0.91	t	7.41	0.91	t	7.41	0.91	t	7.41	0.92	t	7.38	0.92	t	7.41
<b>Daughter</b>															
α	2.99	q	6.51	2.99	q	6.60	u.p.			u.p.					
β	u.p. <sup>[d]</sup>			u.p.			u.p.			u.p.					
γ	1.30	m	7.40	1.30	m	7.39	1.30	m	7.48	1.30	m	7.65			
δ	0.88	t	7.38	0.88	t	7.35	0.88	t	7.35	0.87	t	6.39			

[a] All peaks reported relative to internal standard DSS signal. Chemical shifts δ in ppm and coupling constants J in Hz. [b] A quartet is observed because  $J_{\text{HCH}} \approx J_{\text{HNCH}}$  and the NH proton is not labile and does not undergo fast exchange with solvent, therefore the n + 1 rule approximately holds. [c] The average computed coupling constants  ${}^3J_{\text{HNCH}} = 6.20$  Hz and  ${}^3J_{\text{HCH}} = 7.24$  Hz were calculated with NMR=GIAO at APFD/6-311G\* SCRF = (SMD,water). [d] Abbreviation u.p. stands for under parent peak.

measured immediately after the NMR measurement. The reproducible measurement of pH is easily accomplished with high accuracy so long as one is mindful of the rather long equilibration times.

Table 4 gives the chemical shifts, multiplicity, and coupling constants for the observed signals of the <sup>1</sup>H spectra recorded at the ten pH values studied in the range 7.82 ≤ pH ≤ 11.25. Note that the addition of bicarbonate to these samples causes the α, β, and γ signals to shift downfield by about 0.33 ppm, 0.18 ppm, and 0.04 ppm, respectively, and this shift is independent of pH. At high pH, we report signals for both the parent species (amine and ammonium ion) and the daughter species (carbamate and carbamic acid). With decreasing pH, the intensities of the daughter peaks were diminished and could not be distinguished from noise at pH ≤ 8.70. There are relatively large jumps in the pH measurements from 9.39 to 8.70 and from 8.70 to 7.82 because carbonate has a very poor buffering capacity in that region.

Figure 4 summarizes the results for the quantitative data set over the entire pH range studied. Spectra were scaled such that the highest peak is roughly the same intensity in each spectrum. The intensity of the daughter peaks relative to their respective parent peaks within a spectrum is meaningful (*vide infra*). The relative intensities of the daughter peaks go through a maximum at pH = 10.28.

The multiplicities of the N-attached methylene groups (α signal) differ in the amine and carbamate and the α peaks appear as triplets for the parent amine and as quartets for the daughter carbamate. In the parent butylamine species, the two α hydrogens only couple with the two β hydrogens but not

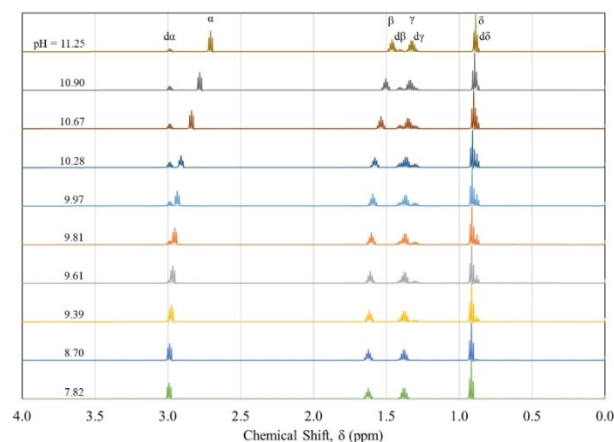


**Figure 4.** Measured <sup>1</sup>H NMR pH profile using the water suppression technique “zgpgppr” for butylamine in 90% H<sub>2</sub>O:10% D<sub>2</sub>O solution with added NaHCO<sub>3</sub>.

with the NH<sub>2</sub> hydrogens, because the latter are exchangeable with solvent water. In contrast, the two α-Hs in the carbamate are coupling with the two β hydrogens as well as the NH hydrogen and the resulting doublet of triplets appears as a quartet. Our assignments were consistent with a correct interpretation of the results of a previous study of carbamylation.<sup>[42]</sup>

The <sup>1</sup>H NMR chemical shifts of butylamine and butylcarbamate are plotted in Figure 5 as a function of pH. Generally, the chemical shifts of the carbamate remain the same over the pH range while the parent peaks shift upfield with increasing pH.

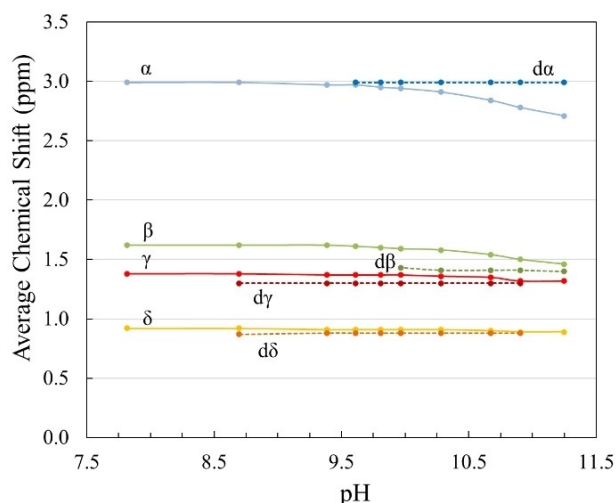


**Figure 5.** Shifts of the  $^1\text{H}$  NMR signals of butylamine and butylcarbamate as a function of pH.

At low pH, the daughter  $\delta$  peak is clearly resolved from the  $\delta$  parent peak, but the daughter  $\alpha$  and  $\beta$  peaks are obscured by the  $\alpha$  and  $\gamma$  parent peaks, respectively. At high pH, the parent  $\alpha$  and  $\gamma$  peaks shift sufficiently upfield and separate from the signals of the  $\alpha$  and  $\beta$  daughter peaks, but the parent  $\delta$  peak begins to overlap with the daughter  $\delta$  peak. Only clearly resolved signals of parent and daughter were used in the quantitative analysis. The  $^{13}\text{C}$  NMR chemical shifts are plotted in Figure S7 in SI1 as a function of pH. The assignment of the butylcarbamate is consistent with one previous report of a biscarbamylated lysine.<sup>[43]</sup>

### pH Profile of KDDE Species in the Capture Reaction

The bulk solution of KDDE was split into ten 10-mL samples and their pH values were adjusted using various aliquots of the base solution. The samples were allowed to equilibrate for approximately 48 hours (Table 3). Once the pH was steady,  $^1\text{H}$  and  $^{13}\text{C}$  NMR spectra were measured.

The  $^1\text{H}$  NMR and  $^{13}\text{C}$  NMR spectra of carbamylated KDDE are shown in Figure 6 and Figure 7. The standard DSS causes peaks at 0.00 ppm (three  $\text{CH}_3$ ), 0.63 ppm ( $\text{Si-CH}_2$ ), 1.76 ppm ( $\text{CH}_2\text{-CH}_2\text{-CH}_2$ ), 2.91 ppm ( $\text{S-CH}_2$ ) ppm in the  $^1\text{H}$  spectra correspond to DSS. The 1.76 ppm peak obscures the Lys  $\beta$  hydrogen peaks and the 2.91 ppm peak begins to overlap with the Lys  $\epsilon$  hydrogen peak at some pH values. DSS also gives peaks in the  $^{13}\text{C}$  NMR at 0 ppm, 18 ppm, 21 ppm, and 57 ppm. The peak at 57 ppm may interfere with the Lys  $\alpha$  daughter peak. The peaks at 120 ppm and 166 ppm in the carbon spectrum correspond to TFA.

Proton assignments were determined using the same procedure as for butylamine with 2D-NMR. Signals for the  $\beta$  hydrogens of Asp-2 and Asp-3 cannot be distinguished. The signals for the Asp  $\beta$  hydrogens are split in both Asp-2 and Asp-3 and give rise to 4 signals. In combination with the HMBC spectroscopy, the order of the signals was determined to be

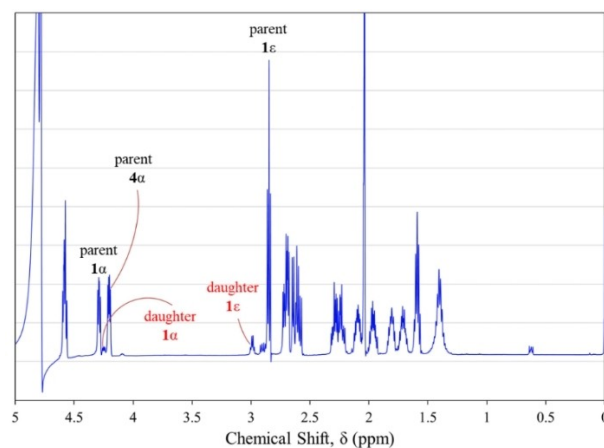


**Figure 6.** Assignment of  $^1\text{H}$  NMR spectrum of carbamylated KDDE.

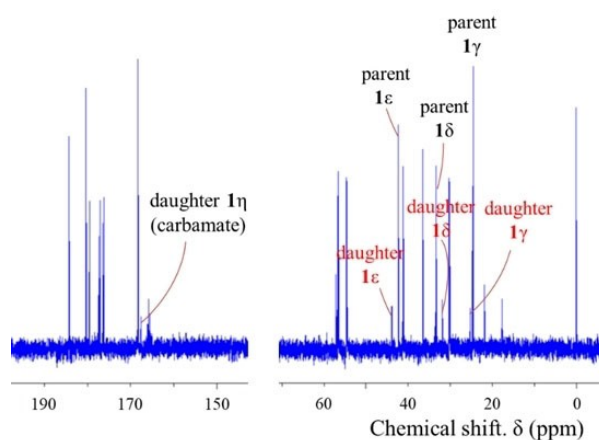


**Figure 7.** Assignment of  $^{13}\text{C}$  NMR spectrum of carbamylated KDDE.

Asp3-Asp2-Asp2-Asp3. Still, the splitting patterns are convoluted, and the shifts are reported together.

The  $^{13}\text{C}$  assignments for the carbonyl carbons were determined with HMBC spectroscopy. All other carbon peaks were assigned with HSQC spectroscopy. The  $\beta$  carbons of Asp-2 and Asp-3 cannot be distinguished because the hydrogen spectrum is unclear.

Figure 8 shows the  $^1\text{H}$  NMR spectra measured for the quantitative data set over the entire pH range studied,  $9.19 \leq \text{pH} \leq 11.18$ . Table 5 summarizes the chemical shift ranges and the multiplicities for the observed signals. The chemical shifts for the  $^1\text{H}$  spectra are plotted in Figure 9 as a function of pH.

### Quantitative Yields of Carbamylation of Butylamine and KDDE as a Function of pH

The integrations of the  $^1\text{H}$  signals were used to determine the daughter/parent ratio  $X$  of the carbamylation, that is, the ratio of the integrals of the daughter and the parent peaks. The daughter/parent ratio  $X$  measured for butylamine and KDDE are

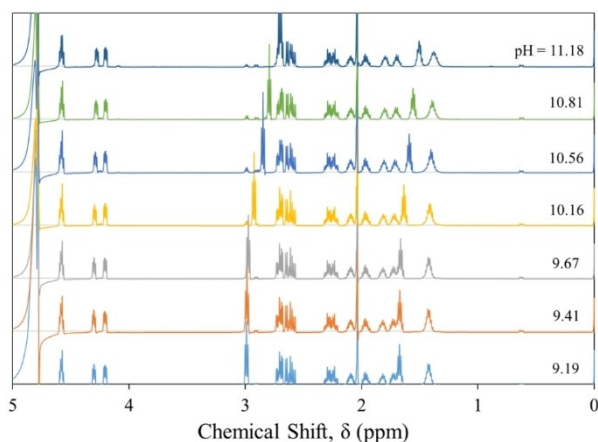


**Figure 8.** Measured  $^1\text{H}$  NMR pH profile using the water suppression technique “zgpgpr” for KDDE in 90%  $\text{H}_2\text{O}$ :10%  $\text{D}_2\text{O}$  solution with added  $\text{NaHCO}_3$ .

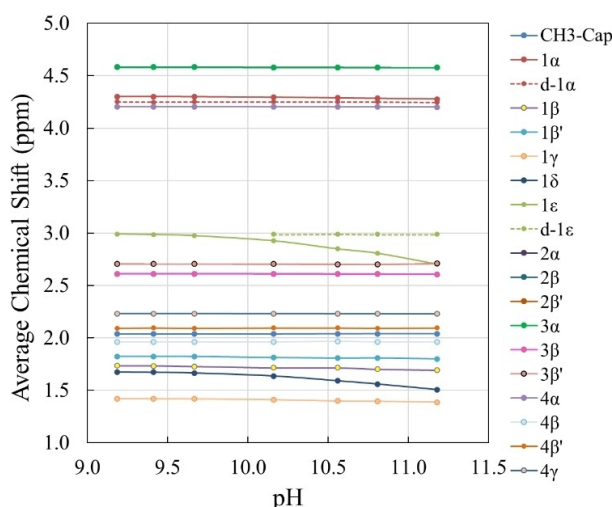


**Figure 9.** Shifts of the  $^1\text{H}$  NMR signals of amine and carbamate species of KDDE as a function of pH.

summarized in Table 6 and Table 7, respectively. The first three columns of each table contain the pH values of the solution, information about which signals were integrated, and the resulting mole fractions of carbamate formed. To avoid confusion, remember that the IUPAC nomenclature of the alkyl chain runs in different directions for butylamine and KDDE's lysine. While the  $\alpha$  signal of butylamine are due to the methylene group directly attached to the carbamate (Scheme 2), the  $\alpha$  signal of lysine refers to the CH peak of the amino acid backbone and the methylene group directly attached to the carbamate gives rise to the  $\epsilon$  signal (Scheme 3).

For butylamine carbamylation, in column 2 of Table 6 are listed those signals that were used for the quantitative analysis based on information about the separability of parent and daughter signals obtained from Figure 4 and Figure 5. At  $\text{pH} \geq 10.90$ , the carbamate mole fraction was determined using the  $\alpha$  and  $\beta$  signals. At pH values 10.28 and 10.67, only the

integrations of the  $\alpha$  signals were used because the daughter  $\beta$  signals started to overlap to the  $\gamma$  signals. The  $\gamma$  signals were not integrated at any case because the parent  $\gamma$  signals overlap with the daughter  $\gamma$  signals and/or daughter  $\beta$  signals. One might not consider the  $\delta$  signal of the terminal methyl groups as a likely messenger of carbamylation at the other end of butylamine. Yet, the parent and daughter signals are well separated below  $\text{pH} = 9.97$ , and at pHs below 9.61, the integration of the  $\delta$  signals is the only way to quantify carbamylation because the  $\alpha$  signals of parent and daughter overlap.

Based on the butylamine study, we had hoped that the signal of the methylene directly attached to the carbamate, the  $\epsilon$  signal in KDDE, would allow for the determination of the carbamate mole fraction. This expectation holds true only for high pH values. At low pH, the parent Lys  $\epsilon$  peak completely overlapped with the daughter peak. It was fortunate that the hydrogen furthest away from the carbamylation site, the  $\alpha$ -CH of the backbone served as an indicator just like the terminal methyl group in butylamine. Therefore, at all pH values, it was possible to determine the mole fraction at least based on the parent:daughter ratio of  $\alpha$  signals. In those cases where it was possible to evaluate both the  $\alpha$  and the  $\epsilon$  signals we found very good agreement of the daughter:parent ratios obtained with the  $\alpha$  or  $\epsilon$  signals only. For best noise averaging, the mole fractions were then computed based on the combination of the  $\alpha$  and  $\epsilon$  signals.

At  $\text{pH} \geq 10.16$ , the Lys  $\epsilon$  parent peaks shift upfield and allow for the clear distinction between the parent Lys  $\epsilon$  and the daughter Lys  $\epsilon$ . At some of the high pH values, the Lys  $\epsilon$  parent signal overlaps with the DSS signal at 2.91 ppm. Thus, Lys  $\epsilon$  and the DSS signal were integrated together, the DSS signal at 0.63 ppm was integrated separately, and the peak integral of the 0.63 ppm signal was subtracted from the total area of the “Lys  $\epsilon$  + DSS” signal to determine the integration for Lys  $\epsilon$ .

Another complication arose because the Lys  $\epsilon$  shifts further upfield and begins to overlap with the Asp  $\beta$  hydrogen peaks at  $\text{pH} = 10.16$  and 10.56. To overcome this issue, a ratio of the areas for the Asp  $\beta$  and Glu  $\gamma$  hydrogen peaks was determined for several spectra and this ratio was found to have a nearly constant value of 0.50. Thus, based on the integration of the Glu  $\gamma$  signal, we were able to determine how much of the area in the Asp  $\beta$  + Lys  $\epsilon$  region was due to the Asp  $\beta$ . This area was subtracted from the integration of the Asp  $\beta$  + Lys  $\epsilon$  region to determine the area attributable to Lys  $\epsilon$ .

The carbamate mole fraction  $Y$  is defined as  $Y = \frac{[\text{daughter}]}{([\text{daughter}] + [\text{parent}])}$  where [daughter] refers to the overall concentration of all  $\text{CO}_2$  adducts and [parent] refers to the overall concentration of all amine species, that is,  $Y = \frac{([\text{carbamic acid}] + [\text{carbamate}])}{([\text{carbamic acid}] + [\text{carbamate}] + [\text{amine}] + [\text{ammonium ion}])}$ . The carbamate mole fraction  $Y$  measures the yield of the carbamylation reactions and the  $Y$  values for both  $\text{BuNH}_2$  and KDDE reactions are plotted as a function of pH in Figure 10. The highest carbamylation yields occur at  $10.2 \leq \text{pH} \leq 10.5$  with only a small difference between butylamine and KDDE. The ratio of the mole fractions of the two systems is  $\text{BuNH}_2:\text{KDDE} = 2.62 \pm 0.19$  averaged over all pH values at which

Table 5. <sup>1</sup>pH Profile (zggppr) of KDDE in 90% H<sub>2</sub>O:10% D<sub>2</sub>O solution with added NaHCO<sub>3</sub>: <sup>1</sup>H NMR spectra.<sup>[a]</sup>

Assign.	pH = 9.19			pH = 9.41			pH = 9.67			pH = 10.16			pH = 10.56			pH = 10.81			pH = 11.18		
	Min	Max	Mult.	Min	Max	Mult.	Min	Max	Mult.	Min	Max	Mult.	Min	Max	Mult.	Min	Max	Mult.	Min	Max	Mult.
CH <sub>3</sub> -Cap	2.04		s	2.04		s	2.04		s	2.04		s	2.04		s	2.04		s	2.04		s
Lys-1																					
1 $\alpha$	4.29	4.31	m	4.29	4.31	m	4.29	4.31	m	4.28	4.31	m	4.27	4.30	m	4.27	4.30	m	4.27	4.29	m
d-1 $\alpha$	4.24	4.26	m	4.24	4.26	m	4.24	4.26	m	4.24	4.26	m	4.24	4.26	m	4.24	4.26	m	4.24	4.25	m
1 $\beta$ (2)	1.72	1.75	m	1.71	1.75	m	1.70	1.75	m	1.68	1.75	m	1.69	1.74	m	1.67	1.73	m	1.66	1.72	m
1 $\gamma$ (2)	1.79	1.85	m	1.79	1.85	m	1.79	1.85	m	1.79	1.84	m	1.78	1.83	m	1.77	1.83	m	1.77	1.83	m
1 $\delta$ (2)	1.39	1.45	m	1.39	1.45	m	1.39	1.45	m	1.38	1.44	m	1.37	1.43	m	1.35	1.45	m	1.35	1.42	m
1 $\epsilon$ (2)	1.65	1.70	m	1.65	1.70	m	1.64	1.69	m	1.61	1.66	m	1.57	1.62	m	1.53	1.58	m	1.48	1.53	m
d-1 $\epsilon$ (2)	2.98	3.00	t	2.97	3.00	t	2.96	2.99	t	2.91	2.94	t	2.84	2.86	t	2.78	2.83	t	2.69	2.72	t
Asp-2																					
2 $\alpha$	4.57	4.60	m	4.57	4.60	m	4.57	4.60	m	4.56	4.60	m									
2 $\beta$ (2)	2.57	2.65	m	2.57	2.65	m	2.57	2.65	m	2.57	2.65	m	2.57	2.65	m	2.57	2.65	m	2.57	2.65	m
2 $\gamma$	2.68	2.73	m	2.68	2.73	m	2.68	2.73	m	2.68	2.73	m	2.68	2.73	m	2.68	2.73	m	2.68	2.74	m
Asp-3																					
3 $\alpha$	4.57	4.60	m	4.57	4.60	m	4.57	4.60	m	4.56	4.60	m									
3 $\beta$ (2)	2.57	2.65	m	2.57	2.65	m	2.57	2.65	m	2.57	2.65	m	2.57	2.65	m	2.57	2.65	m	2.57	2.65	m
3 $\gamma$	2.68	2.73	m	2.68	2.73	m	2.68	2.73	m	2.68	2.73	m	2.68	2.73	m	2.68	2.73	m	2.68	2.74	m
Glu-4																					
4 $\alpha$	4.20	4.22	m	4.19	4.22	m	4.19	4.22	m	4.19	4.22	m	4.19	4.22	m	4.19	4.22	m	4.19	4.21	m
4 $\beta$ (2)	1.93	1.99	m	1.93	1.99	m	1.93	1.99	m	1.93	1.99	m	1.95	1.99	m	1.93	1.99	m	1.93	1.99	m
4 $\gamma$ (2)	2.06	2.13	m	2.07	2.13	m	2.06	2.13	m	2.07	2.12	m	2.07	2.12	m	2.06	2.12	m	2.07	2.12	m
	2.21	2.26	m	2.21	2.26	m	2.21	2.26	m	2.21	2.26	m	2.21	2.26	m	2.20	2.26	m	2.20	2.26	m
	2.27	2.32	m	2.27	2.32	m	2.27	2.32	m	2.27	2.32	m	2.27	2.32	m	2.27	2.32	m	2.27	2.32	m

[a] See footnotes of Table 4.

**Table 6.** Measured daughter/parent ratio, calculated concentrations, and derived free energies for the CO<sub>2</sub> capture reaction by BuNH<sub>2</sub> with [HCO<sub>3</sub><sup>-</sup>]<sub>0</sub> = 68 mM and [Bu-NH<sub>2</sub>]<sub>0</sub> = 45 mM.<sup>[a]</sup>

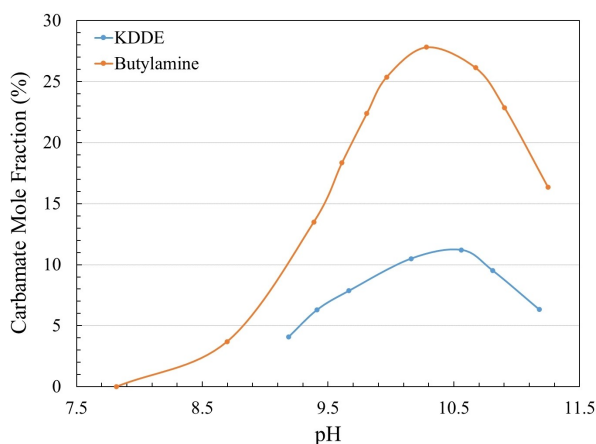
pH	Integrated Peaks	X <sup>(b,c)</sup> [%]	[Bu-NH <sub>2</sub> ]	[Bu-NH-CO <sub>2</sub> H] <sup>[d]</sup>	[Bu-NH-COO <sup>-</sup> ] <sup>[d]</sup>	[CO <sub>2</sub> ] <sup>[f]</sup>	[CO <sub>2</sub> ] <sup>[g]</sup>	I <sup>[d,f]</sup> ΔG <sub>R1</sub>	II <sup>[d,g]</sup> ΔG <sub>R1</sub>	III <sup>[e,f]</sup> ΔG <sub>R1</sub>	IV <sup>[e,g]</sup> ΔG <sub>R1</sub>	
11.25	α, β	16.3	0.0307	0.0320	7.3145	0.0001	0.0001	-1.34	-1.57	-1.54	-1.78	
10.90	α, β	22.9	0.0233	0.1004	10.3458	0.0003	0.0002	-1.33	-1.57	-1.54	-1.77	
10.67	α	26.1	0.0182	0.1948	11.7924	0.0008	0.0005	-1.33	-1.57	-1.54	-1.77	
10.28	α	27.8	0.0108	0.5122	12.6309	0.0033	0.0022	-1.37	-1.60	-1.57	-1.81	
9.97	α, δ	25.4	0.0065	0.9727	11.5601	0.0095	0.0064	-1.43	-1.66	-1.63	-1.87	
9.81	α, δ	22.4	0.0050	1.2312	10.1940	0.0154	0.0104	-1.44	-1.67	-1.64	-1.88	
9.61	δ	18.3	0.0035	1.5872	8.3296	0.0275	0.0185	-1.45	-1.69	-1.66	-1.89	
9.39	δ	13.5	0.0023	1.9520	6.1163	0.0511	0.0344	-1.46	-1.69	-1.66	-1.90	
8.70	δ	3.7	0.0005	2.6050	1.6665	0.2920	0.1968	-1.45	-1.68	-1.65	-1.88	
								Average:	-1.40	-1.63	-1.60	-1.84

[a] Concentrations in mM except for butylcarbamate acid, which is in μM. Energies in kcal/mol. Measurement at pH = 7.817 showed no carbamate signals. [b] Because the daughter species is mostly carbamate at this pH, we use the label "Bu-NH-COO<sup>-</sup>". However, we acknowledge that the NMR signal of the daughter peak may include very small contributions from the protonated form as well. [c] The daughter/parent ratio X is the ratio of the integration of the daughter peak to the integrations of the parent peaks. [d] Using pK<sub>5</sub> = 5.74.<sup>[34]</sup> [e] Using pK<sub>5</sub> = 5.89. [f] Using pK<sub>2</sub> = 6.352.<sup>[33]</sup> [g] Using pK<sub>2</sub> = 6.18.<sup>[45]</sup>

**Table 7.** Measured daughter/parent ratio, calculated concentrations, and derived free energies for the CO<sub>2</sub> capture reaction by KDDE with [HCO<sub>3</sub><sup>-</sup>]<sub>0</sub> = 41 mM and [KDDE]<sub>0</sub> = 10 mM.<sup>[a]</sup>

pH	Integrated Peaks	X <sup>(b,c)</sup> (%)	[Lys-NH <sub>2</sub> ]	[Lys-NH-COOH] <sup>[e]</sup>	[Lys-NH-COO <sup>-</sup> ] <sup>[e]</sup>	[CO <sub>2</sub> ] <sup>[f]</sup>	[CO <sub>2</sub> ] <sup>[g]</sup>	I <sup>[d,f]</sup> ΔG <sub>R1</sub>	II <sup>[d,g]</sup> ΔG <sub>R1</sub>	III <sup>[e,f]</sup> ΔG <sub>R1</sub>	IV <sup>[e,g]</sup> ΔG <sub>R1</sub>	
11.18	α, ε	6.32	0.0071	0.2084	0.4110	0.0001	0.00004	-0.92	-1.15	-1.12	-1.36	
10.81	α, ε	9.53	0.0052	0.1908	0.6347	0.0003	0.0002	-0.93	-1.16	-1.13	-1.37	
10.56	α, ε	11.22	0.0039	0.1324	0.7906	0.0009	0.0006	-0.97	-1.20	-1.17	-1.40	
10.16	α, ε	10.50	0.0021	0.0567	1.0532	0.0035	0.0024	-0.99	-1.23	-1.20	-1.43	
9.67	α	7.87	0.0008	0.0239	1.1188	0.0156	0.0105	-1.17	-1.40	-1.37	-1.61	
9.41	α	6.31	0.0005	0.0115	0.9500	0.0307	0.0207	-1.30	-1.53	-1.50	-1.73	
9.19	α	4.08	0.0003	0.0032	0.6289	0.0546	0.0368	-1.29	-1.52	-1.49	-1.73	
								Average:	-1.08	-1.31	-1.28	-1.52

[a] Concentrations in mM; energies in kcal/mol. [b] Because the daughter species is mostly carbamate at this pH, we use the label "Lys-NH-COO<sup>-</sup>". However, this number reflects the total concentration of the daughter species from the NMR signal. [c] The daughter/parent ratio X is the ratio of the integration of the daughter peak to the integrations of the parent peaks. [d] Using pK<sub>5</sub> = 5.74.<sup>[34]</sup> [e] Using pK<sub>5</sub> = 5.89. [f] Using pK<sub>2</sub> = 6.352.<sup>[33]</sup> [g] Using pK<sub>2</sub> = 6.18.<sup>[45]</sup>

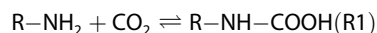
**Figure 10.** Carbamate mole fraction Y as a function of pH of the butylamine and KDDE carbamylation reactions.

measurements were made. This ratio is more of a reflection of the substrate ratio  $S = [\text{HCO}_3^-]_0 / [\text{R-NH}_2]_0$  and the values  $S(\text{BuNH}_2) = 1.51$  and  $S(\text{KDDE}) = 4.1$  and less of the thermochemistry of the carbamylation reaction.

## Thermodynamics of Carbamylation Reactions in Solution

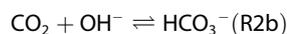
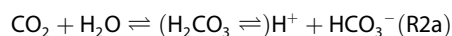
### Multiequilibria Evaluation to Deduce $\Delta G_0$ for the CO<sub>2</sub> Capture Reaction

From the data reported in Table 6, Table 7, and Figure 10, we can determine the  $\Delta G^0$  for the capture reactions at each pH. We describe the formalism for the general case of the capture of CO<sub>2</sub> by alkylamine R-NH<sub>2</sub> to give the alkylcarbamate acid R-NH-COOH, see reaction R1. Equilibrium constants that depend on the nature of the R group are labeled  $K_m(\text{R})$ , where  $m = [1,4,5]$  and R = Bu or R = Lys for the carbamylation studies of butylamine or the lysine in KDDE, respectively.

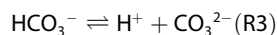


$$K_1(\text{R}) = \frac{[\text{R-NH-COOH}]}{([\text{R-NH}_2][\text{CO}_2])} \quad (1)$$

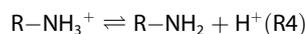
The determination of  $K_1(\text{R})$  is complicated by the fact that each species in reaction R1 engages in pH dependent equilibrium reactions R2–R5.



$$K_2 = \frac{[\text{H}^+][\text{HCO}_3^-]}{[\text{CO}_2]} \quad (2)$$



$$K_3 = \frac{[\text{H}^+][\text{CO}_3^{2-}]}{[\text{HCO}_3^-]} \quad (3)$$



$$K_4(\text{R}) = \frac{[\text{H}^+][\text{R-NH}_2]}{[\text{R-NH}_3^+]} \quad (4)$$



$$K_5(\text{R}) = \frac{[\text{H}^+][\text{R-NH-COO}^-]}{[\text{R-NH-COOH}]} \quad (5)$$

Equation 6 defines the daughter/parent ratio  $X$ , which was measured by integrations for the daughter and parent peaks as described above.

$$X = \frac{[\text{R-NH-COOH}] + [\text{R-NH-COO}^-]}{[\text{R-NH}_2] + [\text{R-NH}_3^+]} \quad (6)$$

With the knowledge of the initial concentration of the amine, the mass balance equation (Eq. 7), and rearrangement of Eq. 4, one can determine  $[\text{R-NH}_2]$  via Eqs. 8 and 9 and  $[\text{R-NH-COOH}]$  via Eq. 10.

$$[\text{R-NH}_2]_0 = [\text{R-NH}_2] + [\text{R-NH}_3^+] + [\text{R-NH-COOH}] + [\text{R-NH-COO}^-] \quad (7)$$

$$\frac{[\text{R-NH}_2]_0}{1+X} = [\text{R-NH}_2] + [\text{R-NH}_3^+] \quad (8)$$

Substituting  $[\text{R-NH}_3^+]$  using the definition of  $K_4(\text{R})$  in Eq. 4, one can solve for the concentration of the amine  $\text{R-NH}_2$ .

$$[\text{R-NH}_2] = \frac{[\text{R-NH}_2]_0}{(1+X)\left(1 + \frac{[\text{H}^+]}{K_4}\right)} \quad (9)$$

Then, using the same amine mass balance equation and the equilibrium quotient for reaction R4, one can solve for the concentration of alkylcarbamic acid.

$$[\text{R-NH-COOH}] = \frac{[\text{R-NH}_2]_0 - [\text{R-NH}_2] - [\text{R-NH}_3^+]}{\left(1 + \frac{K_5}{[\text{H}^+]}\right)} \quad (10)$$

With the concentration of carbamic acid known, it is easy to calculate the concentration of carbamate with Eq. 11.

$$[\text{R-NH-COO}^-] = \frac{K_5 \cdot [\text{R-NH-COOH}]}{[\text{H}^+]} \quad (11)$$

To determine the concentrations of  $\text{HCO}_3^-$ ,  $\text{CO}_3^{2-}$ , and  $\text{CO}_2$ , the mass balance equation (Eq. 12) was employed.

$$[\text{HCO}_3^-]_0 = [\text{HCO}_3^-] + [\text{CO}_2] + [\text{CO}_3^{2-}] + [\text{R-NH-COOH}] + [\text{R-NH-COO}^-] \quad (12)$$

By substitution of the equilibrium quotients  $K_2$  and  $K_3$ , Eq. 12 can be simplified to Eq. 13.

$$[\text{HCO}_3^-] = \frac{[\text{HCO}_3^-]_0 - [\text{R-NHCOOH}] - [\text{R-NH-COO}^-]}{1 + \frac{K_3}{[\text{H}^+]} + \frac{[\text{H}^+]}{K_2}} \quad (13)$$

Then the concentration of  $\text{CO}_2$  can be calculated with Eq. 14.

$$[\text{CO}_2] = \frac{[\text{H}^+] \cdot [\text{HCO}_3^-]}{K_2} \quad (14)$$

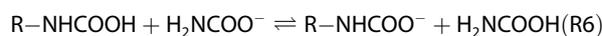
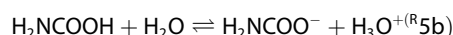
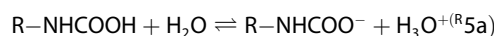
With the concentration of  $\text{R-NH-COOH}$ ,  $\text{R-NH}_2$ , and  $\text{CO}_2$  known,  $K_1$  can be calculated via Eq. 1.

### Equilibrium Constants

The hydrolysis of  $\text{CO}_2$  is described by R2a and R2b and the latter reaction is the dominant pathway for bicarbonate formation at pH above 8.<sup>[44]</sup> The intermediate carbonic acid formation need not be considered in the overall equilibria because the dissociation of the proton ( $\text{p}K_a = 3.7$ )<sup>[33]</sup> and the dehydration reactions are highly favorable for  $\text{H}_2\text{CO}_3$ . For the overall reaction, the  $\text{p}K_2$  value of 6.352<sup>[33]</sup> is commonly used and a slightly lower value of 6.18<sup>[45]</sup> also was reported. Note that the CRC wrongly gives 6.532 as the  $\text{p}K_a$  of the first dissociation of carbonic acid, neglecting the hydration step.<sup>[46]</sup>

The acidity of butylammonium ion was measured<sup>[32]</sup> to be  $\text{p}K_a(\text{Bu}) = 10.6$ , and we employ the same value to approximate  $\text{p}K_a(\text{Lys})$ .

The specific value for the acidity of butylcarbamic acid  $\text{p}K_5(\text{Bu})$  is not reported in the literature. However, the  $\text{p}K_a$  value of aminocarboxylic acid ( $\text{NH}_2\text{COOH}$ ) was determined<sup>[34]</sup> to be  $\text{p}K_5(\text{H}) = 5.74$  ( $T = 273 \text{ K}$ ) and this value can be used in Eq. 10 as a first approximation to obtain  $[\text{Bu-NH-COOH}]$ . However, we studied the effect of adding an alkyl substituent to achieve a better estimate of  $K_5(\text{Bu})$  via the isodesmic<sup>[47]</sup> reaction R6. The direct calculation of acidity of weak acids is notoriously difficult.<sup>[48]</sup> Instead of evaluating R5a and R5b, we are only interested in the computational evaluation of reaction R6 (= R5a–R5b) to determine an R-group correction to the experimentally measured  $\text{p}K_5(\text{H})$  according to Eq. 16.



$$\Delta G(\text{R5a}) = \Delta G(\text{R5b}) + \Delta G(\text{R6}) \quad (15)$$

$$K_5(R5a) = K_5(R5b) \cdot K(R6) = K_{5(R5b)} \cdot \exp(-\Delta G(R6)/RT) \quad (16)$$

To evaluate Eq. 16, we determined the energies of the parent carbamic acid and its carbamate,  $H_2NCOOH$  and  $H_2NCOO^-$ , and of their alkyl substituted analogs,  $R-HNCOOH$  and  $R-HNCOO^-$  ( $R=Me, Et, Pr, Bu$ ) at various levels of density function theory, which we have previously employed in our studies of the  $CO_2$  capture by amine.<sup>[49]</sup> The isodesmic reaction R6 was evaluated for the gas phase and with the solvation model SMD<sup>[50]</sup> with the APFD<sup>[51]</sup> functional and various basis sets. Because the solvation effects are significant, we improved the accuracy of the reaction energies by adding two explicit water molecules to each carbamic acid and carbamate, and details are provided in the supporting information. At our best level, we obtained the reaction energy  $\Delta G_{R6}(Bu) = 0.21$  kcal/mol, which gives  $pK_a(Bu) = 5.89$  for reaction R5a. The  $pK_a(R)$  values of carboxylic acids are 4.76 (Me), 4.87 (Et), 4.83 (Pr), 4.83 (Bu), and 4.85 (Pe),<sup>[52]</sup> and based on their convergence it is well justified to use  $pK_a(Bu) = 5.89$  in the analyses of both the butylamine and the KDDE system.

#### Determination of $\Delta G^0$ values for $CO_2$ Capture by Butylamine and KDDE

For each pH value,  $K_1(R)$  can be calculated from its definition (Eq. 1) with the knowledge of the substrate concentrations  $[CO_2]$  and  $[R-NH_2]$  and the product concentration  $[R-NH-COOH]$ , and the Gibbs free energy for reaction R1 can then be determined using  $\Delta G^0 = -RT \cdot \ln(K_{eq})$ . This evaluation requires multiequilibria analysis together with the initial concentrations  $[HCO_3^-]_0$  and  $[R-NH_2]_0$ , the pH values, and the daughter/parent ratio  $X$  of Table 6 and Table 7.

Both Table 6 and Table 7 contain one column that specifies the amine concentration in the reaction mixture. This amine concentration only depends on the measured daughter/parent ratio  $X$  and the equilibrium constant  $K_4$ . The latter is assumed to be the same for butylamine and KDDE. The specific points included in Figure 1 correspond to the mole fraction  $f(R-NH_2)$  in the measured multi-equilibria for butylamine (red square) and KDDE (yellow circle), respectively. In those pH ranges, the

fractions for  $CO_2$  and carbamate do not noticeably differ from zero and unity, respectively.

Table 6 and Table 7 contain two columns each for the concentration of  $CO_2$  because we employed two values for  $K_2$ . We also calculated the carbamate and carbamic acid concentrations with two  $K_5$  values; the resulting carbamate concentrations are the same in the first four digits and we only report one set the concentrations of carbamate and carbamic acid.

Because of the uncertainties in  $K_2$  and  $K_5$ , we computed  $\Delta G_1$  values with four sets I–IV of  $K_2$  and  $K_5$  combinations. The four sets of  $\Delta G_1(Bu)$  are plotted on the left of Figure 11 as a function of pH and the respective  $\Delta G_1(KDDE)$  are plotted in the same format on the right in Figure 11.

The range of the  $K_2$  and  $K_5$  values both affect  $\Delta G_1$  by about 0.25 kcal/mol. Because  $\Delta G_1$  is lowered by a decrease in  $pK_2$  and an increase in  $pK_5$ , the entire range of likely  $\Delta G_1$  values covers about 0.5 kcal/mol. The  $\Delta G_1$  values for sets I–IV vary with pH and there is a more pronounced increase at higher pH for KDDE. The green shading in Figure 11 indicates the pH range with highest mole fraction  $Y$ . The experimental error associated with  $X$  is minimized for measurements close to maximum carbamylation, that is, at  $pH = 10.28$  for butylamine and at  $pH = 10.56$  for KDDE. Set III is likely to be the most accurate because  $pK_2 = 6.352$  and  $pK_5 = 5.89$  are the best values in our judgement. At those pH values,  $\Delta G_1(Bu) = -1.57$  kcal/mol and  $\Delta G_1(KDDE) = -1.17$  kcal/mol. In anticipation of future re-assessments of the precise values of  $pK_2$  and  $pK_5$ , we present in Figure 12 the  $\Delta G_1$  planes as a function of  $pK_2$  and  $pK_5$ .

## Conclusions

We have demonstrated that the thermochemistry of amine carbamylation in aqueous solution can be quantified by  $^1H$  NMR spectroscopy. This achievement requires the accurate assignment of the  $^1H$  NMR spectra of the amine substrate and the carbamylation product, the exploration of the pH profile of the carbamylation reaction, and the solution of a multi-equilibrium equation system to determine  $\Delta G_1(R)$  for the reaction  $R-NH_2 + CO_2 \rightleftharpoons R-NH-COOH$ .

We developed the NMR approach initially by studying the carbamylation of butylamine. We were able to measure the chemical shifts and relative intensities of butylamine and its

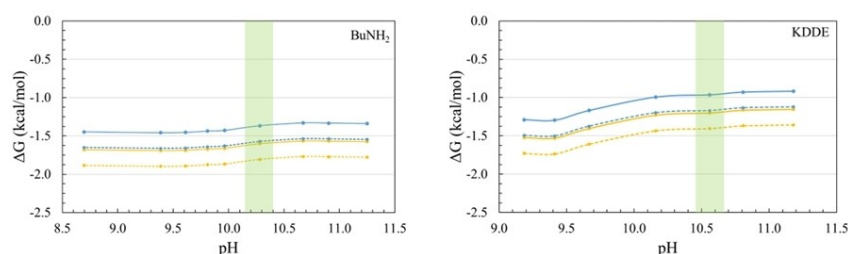


**Figure 11.** Dependence of the Gibbs free energy  $\Delta G_1$  of the capture reaction on pH of the butylamine solution (left) and the KDDE solution (right). Blue:  $pK_2 = 6.352$ ; Yellow:  $pK_2 = 6.18$ ; Solid:  $pK_5 = 5.74$ ; Dashed:  $pK_5 = 5.89$ . Compare Table 6 and Table 7 for scenarios I–IV. We argue that set III (yellow solid) produces the best results.

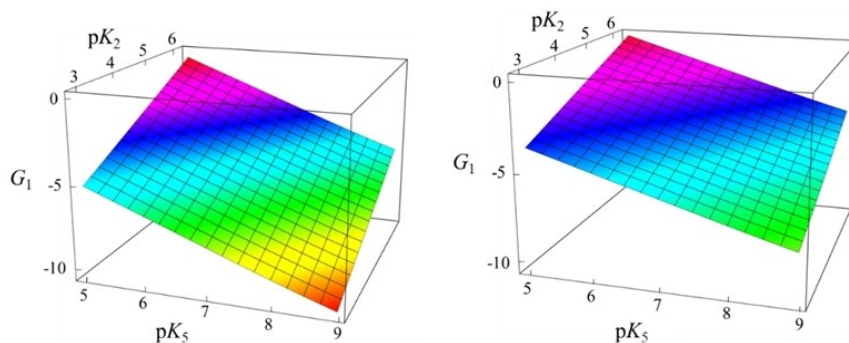


Figure 12. 3D surface of  $\Delta G_1$  relative to  $pK_2$  and  $pK_5$  for butylamine (left) and KDDE (right) measurements.

carbamic acid for a range of pH values and determine the carbamylation yield  $Y$  and the daughter/parent ratio  $X$ . With the protocol established for the study of the carbamylation reaction by NMR spectroscopy, we then turned to the more challenging task of oligopeptide carbamylation at much lower concentration. The oligopeptide KDDE was synthesized, its  $^1\text{H}$  and  $^{13}\text{C}$  NMR spectra were completely assigned, and its carbamylation reaction was also studied as a function of pH in the range of  $8 \leq \text{pH} \leq 11$  to determine the carbamate mole fractions  $Y$  and the daughter/parent ratio  $X$ .

We described the determination of  $\Delta G_1(\text{R})$  by solving the multi-equilibrium equation system with the measurement of the daughter/parent ratio  $X$ , the equilibrium concentration  $[\text{H}^+]$ , the initial concentrations  $[\text{HCO}_3^-]_0$  and  $[\text{R}-\text{NH}_2]_0$ , and the knowledge of the equilibrium constants  $K_m(\text{R})$ ,  $m=2-5$ . Two  $K_2$  values were commonly discussed, the  $K_3$  and  $K_4$  values are well established, and  $K_5$  has not been directly measured to date. We determined the alkylcarbamic acid acidity  $pK_5(\text{R})$  as a function of the R group based on the known acidity of amino carbamic acid  $\text{H}_2\text{N}-\text{COOH}$  and the evaluation of isodesmic reactions with explicit solvent molecules and partial diffuse function to overcome basis set superposition errors. For the reaction energy of the carbamylation of butylamine and KDDE, our best values are  $\Delta G_1(\text{Bu}) = -1.57$  kcal/mol and  $\Delta G_1(\text{KDDE}) = -1.17$  kcal/mol. Both  $\text{CO}_2$  capture reactions are modestly exergonic and thereby ensure reversibility in an energy-efficient manner. These  $\Delta G_1$  values provide strong evidence for the very possibility of reversible  $\text{CO}_2$  capture from air in the presence of water.<sup>[26]</sup> While this carbon capture and release system will neither be fast nor realize high  $\text{CO}_2$  loadings, this biomimetic process offers the distinctive advantage of not requiring external heating. Our simulations have shown that typical temperature differences between night and day suffice to affect reversibility.<sup>[24]</sup>

The  $\text{CO}_2$  capture reaction could be improved by employing amines with lower basicity. In near-neutral aqueous solution, the amino group of lysine in the tetrapeptide will be mostly protonated ( $pK_a \approx 10.4$ ),<sup>[53]</sup> the highest carbamylation yields occur at  $10.2 \leq \text{pH} \leq 10.5$ , and the carbamylation yield is limited by the very low  $\text{CO}_2$  concentration in the range where free amine becomes available. Enzymes have mastered the astounding trick to decrease the  $pK_a$  of the amino group in the lysine

sidechain significantly to 7.9 (Lys166 in *Rhodospirillum rubrum rubisco*),<sup>[54,55]</sup> 5.9 (essential lysine of acetoacetate decarboxylase),<sup>[56]</sup> and even 5.3 (I92 K in *staphylococcal nuclease*).<sup>[57]</sup> The exact value of the  $pK_a$  of Lys201 in spinach rubisco remains unknown. In the absence of the protein envelope of the enzyme active site, one may aim to reduce the basicity of the sidechain amine of the oligopeptide by chemical modification to allow for carbamylation to proceed at a lower pH. It is desirable to access the  $5 \leq \text{pH} \leq 8$  range (grey shading) as shown in the Figure 13, and this line of research is currently being explored.<sup>[58]</sup>

## Experimental Section

For brevity, all the synthetic details and the extensive body of NMR spectra are documented in supporting information, which comes in three parts concerned with butylamine (SI1), KDDE (SI2), and f3 (SI3), respectively.

### NMR Measurements with Water Suppression

NMR spectra were recorded on a 600 MHz Bruker Avance III spectrometer.  $^1\text{H}$ ,  $^{13}\text{C}$  and 2D-NMR spectra were measured at each pH. Water suppression was accomplished by presaturation during the relaxation delay and the mixing time to attenuate the water signal and two pulse programs were employed.<sup>[59]</sup> In a first qualitative set of measurements of butylamine carbamylation, we

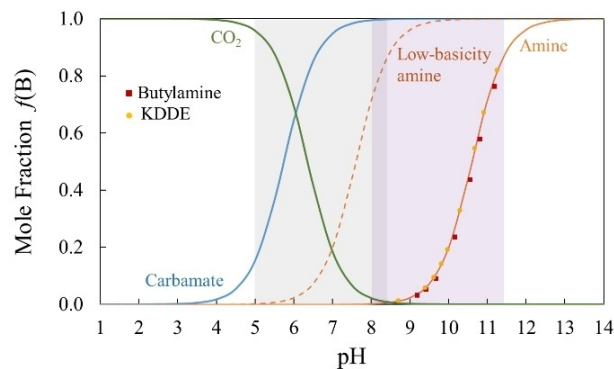


Figure 13. Low basicity amines allow for carbamylation at lower pH and higher  $\text{CO}_2$  concentration.

used the program “noesygppr1d” and the resulting data are given in Supporting Information. The water suppression for the quantitative data sets measured for the carbamylations of butylamine and KDDE was accomplished with the pulse program “zgpgpr”. The transmitter frequency offset was assigned the value of 4.696 ppm, as determined by the chemical shift of the water peak in a preliminary measurement without presaturation. To further minimize the water signal, small sample volumes were used in the NMR tube < 0.5 mL.

### NMR Characterization of Tetrapeptide KDDE

The peptide was synthesized using standard Fmoc solid-phase peptide chemistry on a multiple peptide synthesizer, and experimental details are provided in supporting information SI2. The NMR sample was prepared by adding 5 mg of KDDE peptide to 0.6 mL of a solution consisting of 90% H<sub>2</sub>O and 10% D<sub>2</sub>O. <sup>1</sup>H and <sup>13</sup>C NMR spectra were measured along with a variety of 2D-NMR spectra.

### NMR Characterization of Bridged Oligopeptide DPSG-KDDE-GSPK (“f3”)

Details about the synthesis and NMR spectra recorded for f3 are provided in the Supporting Information SI3. The <sup>1</sup>H and <sup>13</sup>C NMR spectra of f3 in aqueous solution were measured and the spectra are shown in Figure S1 to Figure S4 along with various 2D-NMR spectra of f3 (Figure S5–Figure S13). Assignments were made as with KDDE, and the results are included in Table 1 and Table 2. While it was possible to completely assign all signals of the KDDE portion of f3, there are more overlapping signals in the <sup>1</sup>H NMR spectrum, which makes it impossible to fully assign the DPSG and GSPK sections of the oligopeptide.

### Carbamylation of Butylamine

We introduce HCO<sub>3</sub><sup>−</sup> to the system and rely on the bicarbonate-carbon dioxide equilibrium to generate CO<sub>2</sub> for capture. We collected the qualitative set of NMR data for butylamine immediately after the addition of HCO<sub>3</sub><sup>−</sup> and the quantitative second set was collected after long equilibration times. While carbamate formation is a fast equilibrium, the establishment of the bicarbonate/CO<sub>2</sub> equilibrium is slow, and the solution pH stabilizes only after several hours. The quantitative measurements were used for all thermochemical determinations.

To prepare a sample for the carbamylation measurements, 2.25 mL (22.7 mmol) of butylamine was added to 97.75 mL of 90% H<sub>2</sub>O:10% D<sub>2</sub>O solution. Then, 1.9125 g (22.77 mmol) of NaHCO<sub>3</sub> was added to the solution. Finally, 12 mg of DSS (sodium 4,4-dimethyl-4-silapentane-1-sulfonate; sodium trimethylsilylpropane-sulfonate) was added to the bulk solution as an internal standard. The pH of the sample solutions was measured with an Accumet AP115 pH meter.

### Carbamylation of KDDE

The measurement of the carbamylation reaction of KDDE followed the protocol developed for butylamine, but the sample concentration of the oligopeptide was roughly 1/30 of the butylamine concentration. To observe sufficient carbamylation at these low amine concentrations, we increased the bicarbonate/KDDE ratio. Thus, 0.3965 g (0.726 mmol) of KDDE was added to 72 mL of 90% H<sub>2</sub>O:10% D<sub>2</sub>O solution. The pH of solution was increased to ca. 8.45 with 3 M NaOH. Bicarbonate (2.92 mmol) was added to achieve

a bicarbonate/KDDE ratio of about 4. A small aliquot of internal standard DSS was added; <sup>1</sup>H NMR signals [ppm]: 0.00, 0.63, 1.78, 2.91; <sup>13</sup>C NMR signals [ppm]: 0.00, 17.64, 21.75, 57.02.

## Supporting Information Summary

More detailed data and spectra are available in the Supporting Information. This paper comes with three sets of Supporting Information. Supporting Information 1 contains all the butylamine related contents. Supporting Information 2 contains the experimental details of the synthesis of the KDDE tetrapeptide together with its 1D- and 2D-NMR spectra. Supporting Information 3 contains the experimental details of the synthesis of the bridged oligopeptide DPSG-KDDE-GSPK (“f3”) together with its 1D- and 2D-NMR spectra. Additional references cited within the Supporting Information.<sup>[60–83]</sup>

## Acknowledgements

We thank Prof. Dr. Michael Reithofer, Universität Wien, for chemical synthesis of KDDE employed in preliminary studies. This work was supported by grant #1665487 from the National Science Foundation.

## Conflict of Interest

The authors declare no conflict of interest.

## Data Availability Statement

The data that support the findings of this study are available in the supplementary material of this article.

**Keywords:** amine · CO<sub>2</sub> absorption · multi-equilibrium system · oligopeptide · Rubisco

- [1] Trends in Atmospheric Carbon Dioxide, US Department of Commerce, National Oceanic & Atmospheric Administration (NOAA), Earth System Research Laboratory, Global Monitoring Division. Available online: <http://www.esrl.noaa.gov/gmd/ccgg/trends> (accessed on January 5<sup>th</sup>, 2023).
- [2] Trends in Atmospheric Carbon Dioxide, US Department of Commerce, National Oceanic & Atmospheric Administration (NOAA), Earth System Research Laboratory, Global Monitoring Division. Available online: <https://www.esrl.noaa.gov/gmd/ccgg/trends/global.html#global> (accessed on January 5<sup>th</sup>, 2023).
- [3] D. W. Keith, *Science* **2009**, 325, 1654–1655.
- [4] S. Solomon, G. K. Plattner, R. Knutti, P. Friedlingstein, *Proc. Nat. Acad. Sci.* **2009**, 106, 1704–1709.
- [5] T. Gasser, G. Guivarch, K. Tachiiri, C. D. Jones, P. Ciais, *Nat. Commun.* **2015**, 6, 7958.
- [6] J. Hansen, M. Sato, P. Kharecha, K. von Schuckmann, D. J. Beerling, J. Cao, S. Marcott, V. Masson-Delmotte, M. J. Prather, E. J. Rohling, J. Shakun, P. Smith, A. Laci, G. Russell, R. Ruedy, *Earth Syst. Dynam.* **2017**, 8, 577–616.

- [7] E. S. Sanz-Perez, C. R. Murdock, S. A. Didas, C. W. Jones, *Chem. Rev.* **2016**, *116*, 11840–11876.
- [8] N. McQueen, K. V. Gomes, C. McCormick, K. Blumanthal, M. Pisciotta, J. Wilcox, *Prog. Energy* **2021**, *3*, 032001.
- [9] P. Smith, S. J. Davis, F. Creutzig, S. Fuss, J. Minx, B. Gabrielle, E. Kato, R. B. Jackson, A. Cowie, E. Kriegler, D. P. van Vuuren, J. Rogelj, P. Ciaia, J. Milne, J. G. Canadell, D. McCollum, G. Peters, R. Andrew, V. Krey, G. Shrestha, P. Friedlingstein, T. Gasser, A. Grübler, W. K. Heidug, M. Jonas, C. D. Jones, F. Kraxner, E. Little, J. R. Lowe, J. R. Moreira, N. Nakicenovic, M. Obersteiner, A. Patwardhan, M. Rogner, E. Rubin, A. Sharifi, A. Torvanger, Y. Yamagata, J. Edmonds, C. Yongsung, *Nat. Clim. Change* **2016**, *6*, 42–50.
- [10] J. Tollefson, *Nature* **2018**, *558*, 173.
- [11] V. Gutknecht, S. O. Snæbjörnsdóttir, B. Sigfússon, E. S. Aradóttir, L. Charles, *Energy Procedia* **2018**, *146*, 129–134.
- [12] S. Fuss, J. G. Canadell, G. P. Peters, M. Tavoni, R. M. Andrew, P. Ciaia, R. B. Jackson, C. D. Jones, F. Kraxner, N. Nakicenovic, C. Le Quééré, M. R. Raupach, A. Sharifi, P. Smith, Y. Yamagata, *Nat. Clim. Change* **2014**, *4*, 850–853.
- [13] E. S. Sanz-Pérez, C. R. Murdock, S. A. Didas, C. W. Jones, *Chem. Rev.* **2016**, *116*, 11840–11876.
- [14] C. Faurholt, *J. Chim. Phys. Phys.-Chim. Biol.* **1925**, *22*, 1–44.
- [15] F. J. W. Roughton, *Physiol. Rev.* **1935**, *15*, 241–296.
- [16] F. J. W. Roughton, V. H. Booth, *Biochem. J.* **1938**, *32*, 2049–2069.
- [17] W. C. Stadie, H. O'Brien, *J. Biol. Chem.* **1936**, *112*, 723–758.
- [18] W. C. Stadie, H. O'Brien, *J. Biol. Chem.* **1937**, *117*, 439–470.
- [19] X. Yang, R. J. Rees, W. Conway, G. Puxty, Q. Yang, D. Winkler, *Chem. Rev.* **2017**, *117*, 9524–9593.
- [20] L. J. Kim, R. L. Siegelman, H. Z. H. Jiang, A. C. Forse, J. H. Lee, J. D. Martell, P. J. Milner, J. M. Falkowski, J. B. Neaton, J. A. Reimer, *Science* **2020**, *24*, 392–396.
- [21] W. Zheng, Z. Yan, R. Zhang, W. Jiang, X. Luo, Z. Liang, Q. Yang, H. Yu, *Chem. Eng. Sci.* **2022**, *251*, 117452.
- [22] X. Yang, R. J. Rees, W. Conway, G. Puxty, Q. Yang, D. A. Winkler, *Chem. Rev.* **2017**, *117*, 9524–9593.
- [23] P. V. Kortunov, M. Siskin, L. S. Baugh, D. C. Calabro, *Energy Fuels* **2015**, *29*, 5919–5939.
- [24] A. Muelleman, J. Schell, S. Glaser, R. Glaser, *C* **2016**, *2*, 18.
- [25] R. Glaser, Chapter 11 in *Advances in CO<sub>2</sub> Capture, Sequestration and Conversion* (Eds: F. Jin, L. N. He, Y. H. Hu), ACS Symposium Series; American Chemical Society: Washington, D. C., 2015, pp. 265–293.
- [26] R. Glaser, P. O. Castello-Blind, J. Yin, Chapter 17 in *New and Future Developments in Catalysis, Activation of Carbon Dioxide* (Eds: S. L. Suib), Elsevier: Amsterdam, Netherlands, 2013, pp. 501–534.
- [27] U. Feller, I. Anders, T. Mae, *J. Exp. Bot.* **2008**, *59*, 1615–1624.
- [28] T. C. Taylor, I. Andersson, *Biochemistry* **1997**, *36*, 4041–4046.
- [29] W. W. Cleland, T. J. Andrews, S. Gutteridge, F. C. Hartman, G. H. Lorimer, *Chem. Rev.* **1998**, *98*, 549–561.
- [30] G. H. Lorimer, M. R. Badger, T. J. Andrews, *Biochemistry* **1976**, *15*, 529–536.
- [31] B. Dutcher, M. Fan, A. Russell, *ACS Appl. Mater. Interfaces* **2015**, *7*, 2137–2148.
- [32] D. H. Everett, B. R. W. Pinsent, *Proc. R. Soc. London Ser. A* **1952**, *215*, 416–429.
- [33] B. H. Gibbons, J. T. Edsall, *J. Biol. Chem.* **1963**, *238*, 3502–3507.
- [34] F. J. W. Roughton, *J. Am. Chem. Soc.* **1941**, *63*, 2930–2934.
- [35] J. Keeler, in *Understanding NMR Spectroscopy*, 2<sup>nd</sup> ed., Wiley: Hoboken, NJ, 2010; pp.221–225. ISBN 978-0-470-74608-0.
- [36] E. Pretsch, P. Bühlmann, M. Badertscher, in *Structure of Organic Compounds: Tables of Spectral Data*, 4<sup>th</sup> ed.; Springer: Berlin, 2009.
- [37] J. Keeler, in *Understanding NMR Spectroscopy*, 2<sup>nd</sup> ed.; Wiley: Hoboken, NJ, 2010; pp.281–284. ISBN 978-0-470-74608-0.
- [38] J. Keeler, in *Understanding NMR Spectroscopy*, 2<sup>nd</sup> ed.; Wiley: Hoboken, NJ, 2010; pp.212–214. ISBN 978-0-470-74608-0.
- [39] J. Keeler, in *Understanding NMR Spectroscopy*, 2<sup>nd</sup> ed.; Wiley: Hoboken, NJ, 2010; pp.215–219. ISBN 978-0-470-74608-0.
- [40] J. Keeler, in *Understanding NMR Spectroscopy*, 2<sup>nd</sup> ed.; Wiley: Hoboken, NJ, 2010; pp.220–221. ISBN 978-0-470-74608-0.
- [41] NDBS No. 1091. [http://sdfs.db.aist.go.jp/sdfs/cgi-bin/direct\\_frame\\_top.cgi](http://sdfs.db.aist.go.jp/sdfs/cgi-bin/direct_frame_top.cgi).
- [42] M. George, R. G. Weiss, *Langmuir* **2003**, *19*, 8168–8176.
- [43] J. S. Morrow, P. Keim, F. R. N. Gurd, *J. Biol. Chem.* **1974**, *240*, 7484–7494.
- [44] X. Wang, W. Conway, R. Burns, N. McCann, M. Maeder, *J. Phys. Chem. A* **2010**, *114*, 1734–1740.
- [45] J. S. Morrow, P. Keim, F. R. N. Gurd, *J. Biol. Chem.* **1974**, *240*, 7484–7494.
- [46] *CRC Handbook of Chemistry and Physics*, 89<sup>th</sup> ed. (Eds: D. R. Lide), CRC Press: Boca Raton, FL, **2008**; Section 8.
- [47] IUPAC. Compendium of Chemical Terminology, 2<sup>nd</sup> ed. (the “Gold Book”). Compiled by A. D. McNaught and A. Wilkinson. Blackwell Scientific Publications, Oxford (1997). Online version (2019–) created by S. J. Chalk. ISBN 0-9678550-9-8.
- [48] B. Thapa, H. B. Schlegel, *J. Phys. Chem. A* **2017**, *121*, 4698–4706.
- [49] J. Schell, K. Yang, R. Glaser, *J. Phys. Chem. A* **2021**, *125*, 9578–9593.
- [50] A. V. Marenich, C. J. Cramer, D. G. Truhlar, *J. Phys. Chem. B* **2009**, *113*, 6378–6396.
- [51] A. Austin, G. Petersson, M. J. Frisch, J. Dobek, G. Scalmani, K. Throssell, *J. Chem. Theory Comput.* **2012**, *8*, 4989–5007.
- [52] Dissociation Constants of Organic Acids and Bases, in *CRC Handbook of Chemistry and Physics*, 88<sup>th</sup> Edition (Eds: D. R. Lide), CRC Press: Boca Raton, FL, **2007**; pp 8–42 to 8–46.
- [53] Y. Nozaki, C. Tanford, *Methods Enzymol.* **1967**, *11*, 715–734.
- [54] F. C. Hartman, S. Milanez, E. H. Lee, *J. Biol. Chem.* **1985**, *260*, 13968–13975.
- [55] D. E. Van Dyk, J. V. Schloss, *Biochemistry* **1986**, *25*, 5145–5159.
- [56] D. E. Schmidt, F. H. Westheimer, *Biochemistry* **1971**, *10*, 1249–1253.
- [57] D. G. Isom, C. A. Castaneda, B. R. Cannon, B. Garcia-Moreno, *PNAS* **2011**, *108*, 5260–5265.
- [58] B. Jameson, R. Glaser, *ChemSelect* **2022**, *7*, e202203132.
- [59] R. L. McKay, *Concepts Magn. Reson. Part A* **2011**, *38*, 197–220.
- [60] B. H. Gibbons, J. T. Edsall, *J. Biol. Chem.* **1963**, *238*, 3502–3507.
- [61] H. S. Harned, R. Davis Jr., *J. Am. Chem. Soc.* **1943**, *65*, 2030–2037.
- [62] J. S. Morrow, P. Keim, F. R. N. Gurd, *J. Biol. Chem.* **1974**, *240*, 7484–7494.
- [63] F. J. W. Roughton, *Physiol. Rev.* **1935**, *15*, 241–296.
- [64] F. J. W. Roughton, V. H. Booth, *Biochem. J.* **1938**, *32*, 2049–2069.
- [65] W. C. Stadie, H. O'Brien, *J. Biol. Chem.* **1936**, *112*, 723–758.
- [66] W. C. Stadie, H. O'Brien, *J. Biol. Chem.* **1937**, *117*, 439–470.
- [67] F. Barzagli, F. Mani, F. M. Peruzzini, *Int. J. Greenhouse Gas Control* **2011**, *5*, 448–456.
- [68] Q. Yang, A. Ali, D. Winkler, G. Puxty, M. Attalla, *Energy Procedia* **2009**, *1*, 955–962.
- [69] F. Mani, M. Peruzzini, P. Stoppioni, *Green Chem.* **2006**, *8*, 995–1000.
- [70] H. F. Svendsen, A. F. Ciftja, A. Hartono, *Int. J. Greenhouse Gas Control* **2013**, *16*, 224–232.
- [71] M. George, R. G. Weiss, *Langmuir* **2003**, *19*, 8168–8176.
- [72] W. Gombler, *Z. Naturforsch.* **1986**, *36b*, 1561–1565.
- [73] M. Nakahara, S. Morooka, C. Wakai, N. Matubayasi, *J. Phys. Chem. A* **2005**, *109*, 6610–6619.
- [74] J. S. Morrow, P. Keim, F. R. N. Gurd, *J. Biol. Chem.* **1974**, *240*, 7484–7494.
- [75] Gaussian 16, Revision A.03, M. J. Frisch, G. W. Trucks, H. B. Schlegel, G. E. Scuseria, M. A. Robb, et al. Gaussian, Inc., Wallingford CT, 2016.
- [76] A. Austin, G. Petersson, M. J. Frisch, J. Dobek, G. Scalmani, K. Throssell, *J. Chem. Theory Comput.* **2012**, *8*, 4989–5007.
- [77] J. Schell, K. Yang, R. Glaser, *J. Phys. Chem. A* **2021**, *125*, 9578–9593.
- [78] A. D. Mclean, G. S. Chandler, *J. Chem. Phys.* **1980**, *72*, 5639–5648.
- [79] K. Raghavachari, J. S. Binkley, R. Seeger, J. A. Pople, *J. Chem. Phys.* **1980**, *72*, 650–654.
- [80] M. J. Frisch, A. Pople, J. S. Binkley, *J. Chem. Phys.* **1984**, *80*, 3265–3269.
- [81] A. V. Marenich, C. J. Cramer, D. G. Truhlar, *J. Phys. Chem. B* **2009**, *113*, 6378–6396.
- [82] R. M. Balabin, *J. Chem. Phys.* **2008**, *129*, 164101.
- [83] Dissociation constants of organic acids and bases. In *CRC Handbook of Chemistry and Physics*, 88<sup>th</sup> Edition; D. R. Lide, Eds.; CRC Press: Boca Raton, FL, **2007**; pp 8–42 to 8–46.

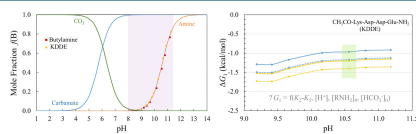
Manuscript received: January 20, 2023

Revised manuscript received: February 23, 2023

Version of record online: ■■■

# RESEARCH ARTICLE

**Rubisco-mimetic capture and release (CCR) systems are described for reversible CO<sub>2</sub> capture from air. The thermochemistry of carbamylation of KDDE-type oligopeptides was determined in aqueous solution.**



*Dr. K. Yang, Dr. J. Schell, Dr. F. Gallazzi,  
Dr. W. Wycoff, Prof. R. Glaser\**

1 – 15

**NMR Study of CO<sub>2</sub> Capture by Butylamine and Oligopeptide KDDE in Aqueous Solution: Capture Efficiency and Gibbs Free Energy of the Capture Reaction as a Function of pH**

